Pergamon

Int. J. Heat Mass Transfer. Vol. 37, No. 17, pp. 2687–2698, 1994

0017-9310/94 $7.00 + 0.00

0017-9310(94)E0080-E

Experimental study of three-dimensional natural convection in enclosures with different working fluids

SHOU-SHING HSIEH and CHIH-YAO WANG

Department of Mechanical Engineering, National Sun Yat-Sen University, Kaohsiung, Taiwan 80424, Republic of China

(*Received* 19 *July* 1993 *and in final form* 11 *March* 1994)

Abstract—This paper presents an experimental study for buoyancy-induced natural convection in the Rayleigh number range of 8.7×10^2–2.0×10^9 inside rectangular enclosures wherein the two vertical walls were heated on the right wall and cooled on the left wall, respectively. The remaining four walls are adiabatic. Temperature data were taken for aspect ratios of $1 \leqslant A \leqslant 20$ and Prandtl numbers of $0.7 \leqslant Pr \leqslant 464$. To gather detailed information regarding flow and heat transfer measurements, flow visualization as well as qualitative information of thermal fields (only for $8.7 \times 10^2 \leqslant Ra \leqslant 1.5 \times 10^4$) using holographic techniques were made and analysed. Results are presented for a range of Rayleigh numbers, Prandtl numbers and for various values of the aspect ratio. Furthermore, thermal correlations as a function of Rayleigh numbers and geometrical parameters and working fluids for different flow regimes were developed, which were also qualitatively verified by existing results.

1. INTRODUCTION

BUOYANCY-DRIVEN flows in enclosures with differentially heated vertical walls have been a topic of continuing interest because of their applications in a number of areas, such as heating and cooling of buildings, cryogenic storage tanks, the cooling of electronic components and solar energy collectors, and because of their fundamental importance. Extensive reviews of the work are given by Ostrach [1, 2] and Bejan [3].

Although studies have been reported focusing on triangular [4] and spherical enclosures [5], most of the basic research on natural convection in enclosures has centered on rectangular and cylindrical enclosures. Although there have been a number of analytical, numerical and experimental studies for low to moderate values of the Rayleigh number that comprise laminar flow, far fewer studies have been reported for high Rayleigh number transitional and turbulent flows. Heat is transferred from the hot to the cold wall essentially by conduction when the Rayleigh number is small or moderately large. For large Rayleigh numbers, a core of uniform temperature and vorticity was assumed to exist in the central region of the enclosure, surrounded by a continuous boundary layer.

It is obvious that convective flows, as well as fluid motion in general, are three-dimensional. There are very few articles in the literature on three-dimensional flow in enclosures with differential side heating. A three-dimensional numerical study of this problem was presented by de Vahl Davis [6]. Their calculation confirms that the existence of secondary roll is an effect of dominating convection. Based on their calculations, the flow field in the enclosure appears strongly three-dimensional, with spiraling streamlines transporting fluid from the core to the side walls and back. Recently, Fusegi *et al.* [7] reported a numerical work of three-dimensional natural convection in a differentially heated cubical enclosure for $10^3 \leqslant Ra \leqslant 10^6$. Gadgil *et al.* [8] numerically calculated a hot wall average Nusselt number of 145% for a cube with one of its vertical surfaces maintained at a more uniform temperature than the other five surfaces at $Ra = 1.15 \times 10^{10}$.

Sadowski *et al.* [9] presented an investigation of the phenomenon of three-dimensional natural convection inside a rectangular cavity driven by a single vertical wall with a warm and cold region. Their results showed that, apart from the region near the vertical driving wall and along the adjoining top and bottom surfaces close to the driving wall, the temperature field is remarkably two-dimensional, linearly stratified in the vertical direction. The fluid in the remainder of the enclosure is practically stagnant. A three-dimensional steady-flow structure of natural convection in a cube cavity with two opposite vertical walls kept at prescribed temperatures was investigated experimentally by Hiller *et al.* [10]. More recently, Lankhorst *et al.* [11] conducted an experiment on buoyancy-driven flows in a differentially heated air-filled square enclosure in the high Rayleigh number range of 1×10^9–4×10^9. Velocity data were obtained through LDV measurements. Although most of the experimental investigations of natural convection in an enclosure with a high aspect ratio assume that the flow field is two-dimensional, it is essentially necessary to under-

NOMENCLATURE

A	aspect ratio, H/L
$\bar{A}$	area of wall [m^2]
C	specific heat [J kg^{-1} K^{-1}]
g	acceleration of gravity [m s^{-2}]
Gr	Grashof number $g\beta(T_H-T_C)H^3/\nu^2$
h	heat transfer coefficient [W m^{-2} K^{-1}]
H	height of slot [m]
k	thermal conductivity [W m^{-1} K^{-1}]
L	width of slot [m]
$\dot{m}$	mass rate of isothermal tank [kg s^{-1}]
Nu	Nusselt number, hL/k
Pr	Prandlt number, ν/α
q	non-dimensional temperature, $T-T_C/T_H-T_C$
q	heat flux [W m^{-2}]
Q	heat transfer rate [W]
Ra	Rayleigh number, $g\beta(T_H-T_C)H^3/\nu\alpha$
Ra_y	local Rayleigh number, $g\beta(T_w-T_m)y^3/\nu\alpha$
S	lateral aspect ratio, W/L
T	temperature [K]
W	length of slot [m]
x	direction parallel to the width of the slot [m]
y	direction parallel to the height of the slot [m]
z	direction parallel to the length of the slot [m].

Greek symbols

α	thermal diffusivity of fluid [m^2 s^{-1}]
β	thermal expansion coefficient [K^{-1}]
ν	kinematic viscosity of fluid [m^2 s^{-1}]
ρ	density of fluid [kg m^{-3}].

Subscripts

C	cold wall
H	hot wall
m	reference mean bulk temperature, $(T_H+T_C)/2$
w	vertical wall
y	distance from leading edge.

stand experimentally the form or significance of the three-dimensional effects occurring in a real flow.

This paper addresses the problem of three-dimensional natural convection in rectangular enclosures with differentially heated vertical walls and with different working fluids, as shown in Fig. 1. To isolate the effect of these two heated and cooled vertical walls, the remaining four walls are adiabatic. The aim of this research is to determine the natural convection heat transfer and flow pattern induced in the enclosures. Air, water and silicone oil were the working fluids and the experiments were conducted in moderate and high Rayleigh number regimes (1.0×10^6–2.0×10^9) characteristic of natural convection in buildings. The temperature fields within the enclosures were obtained, and flow as well as thermal visualization were achieved by adding neutrally buoyant reflective suspended aluminum particles to the fluids and passing a sheet of laser light through the enclosure. Since three-dimensional measurements are relatively scarce, the data should be useful in three-dimensional numerical code validation and the assessment of the assumption of two-dimensionality in previous experiments with high aspect ratios. Moreover, it is worthwhile noting that, based on the present study, the extent of the applicability of the earlier two-dimensional results to actual three-dimensional systems was explored.

2. EXPERIMENTAL SET-UP AND PROCEDURE

2.1. *Experimental facility*

The thermal convection flow was generated in $100\times20\times60$ mm, $100\times20\times100$ mm and $100\times20\times200$ mm rectangular enclosures. Figure 2 shows the enclosure and the coordinate system used. The y-direction is vertically upwards. Two opposite lateral walls of the box ($x=0$ and $x=L$) were made

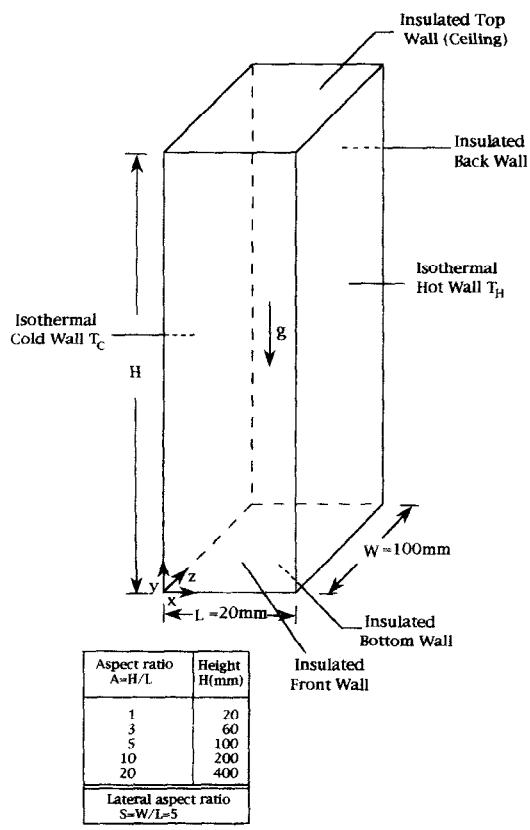

FIG. 1. Schematic of physical and coordinate system.

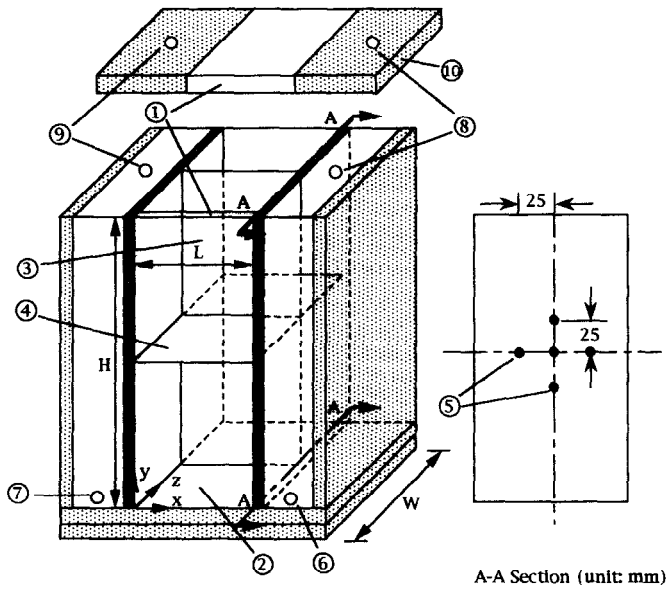

(1) test section
(2) 10mm plexiglass
(3) the vertical(xy) plane at z=W/2
(4) the horizontal(xz) plane at y=H/2
(5) wall temperature measurement position(at two opposite vertical walls)
(6) hot water inlet
(7) cold water inlet
(8) hot water outlet
(9) cold water outlet
(10) top ceiling of the enclosure

10mm thickness polystyrene foam thermal insulator
6mm thickness copper plate

FIG. 2. Schematic of test section.

of copper (6 mm thickness) and kept at a prescribed constant temperature by two isothermal baths. The other four walls, made from 10 mm plexiglass with 10 mm polystyrene foam, were considered to be thermal insulators when temperature measurements were conducted. The great thermal capacity and thermal conductivity of the copper walls allowed us to maintain constant and uniform temperatures of the heated and cooled walls. These temperatures were continuously measured by means of copper/constantan thermocouples (AWG 28) and recorded by a Solartron ORION A automatic data acquisition system. The observed temperature fluctuations were less than 0.2°C. Heating and cooling of the vertical isothermal walls is accomplished by pumping hot demineralized water at temperature T_H and cold demineralized water at temperature T_C through the double-paned walls. The water is circulated and regulated through commercially available constant temperature baths. Suitable values of T_H and T_C were chosen to minimize the temperature difference between the mean enclosure temperature and the ambient. The temperature differences between the heated and cooled walls was varied in the range between 0.5 and 80°C. The ambient temperatures were kept at 25°C. The enclosure was filled with air, water and silicone oil as working fluids for each experimental run.

Five copper/constantan thermocouples were installed at various locations on each of the two (heated/cooled) vertical walls. The maximum temperature deviation from the mean temperature of the wall was ± 0.1°C. All thermocouples were connected to a data acquisition/control unit. The data logger in turn was connected to a personal computer. Wall temperature measurements were taken and averaged arithmetically to obtain T_H and T_C at each steady state. From these, $\Delta T (T_H - T_C)$ values required to calculate the Rayleigh and Nusselt numbers were obtained. The ambient temperature was constantly monitored. The accuracy of all thermocouple measurements was ± 0.2°C. Thermal conditions were stable to within ± 0.1°C over the measurement period. A very thin (AWG 40) thermocouple probe was inserted through a slot in the top ceiling of the enclosure, approximately in the middle of the vertical sides, and traversed in the horizontal or vertical direction to measure the local temperature of the core. This probe was carefully shifted or lowered to a desired position or depth and held there for 5 min to assure that any flow disturbance had died away. Temperature measurements were thus taken, and the probe was shifted or lowered further until eventually the left vertical wall or bottom wall was reached.

2.2. *Flow/thermal visualization*

Flow structures were visualized using photographic records of the motion of tracer particles illuminated

by a sheet of white light. Aluminum powders were used as tracer particles. The typical size of the particles was 5–15 μm and their concentration in the working fluid was kept below 0.1% by weight. Time-exposure (25–35 s) photographs were taken of the flow patterns using Cannon-AE1 camera with FUJI COLOR ISO 1600 films.

In addition, for further understanding of the thermal characteristics of the study, laser holographic interferometry was used. It is essentially similar to that described by Aung and O'Regan [12] and is shown schematically in Fig. 3. Coherent light (632.8 nm) from a 35 mW Spectra-Physics Model 124-B He–Ne laser split into an object beam and a reference beam was expanded to a 90 mm planar wave via a $\times 20$ microscopic objective and $\times 40$ microscopic objective and two collimating lenses (diameter 12.7 cm). Pinholes of 20 mm diameter were located at the focal point of the microscopic objectives in order to eliminate intensity variations in the wave fronts intersecting at the photographic plate (here at an angle of 60°) and to produce a hologram when the photographic emulsion was exposed simultaneously to the two beams and then developed *in situ*. The interferometer components and test section were mounted securely to a 1.4×2.0 m vibration-free optical table.

3. DATA REDUCTION AND UNCERTAINTY

The local values of the thermophysical properties of the working fluid in the enclosure were obtained at a reference temperature referred to as a mean bulk temperature of

$$T_m = 0.5(T_H + T_C).$$

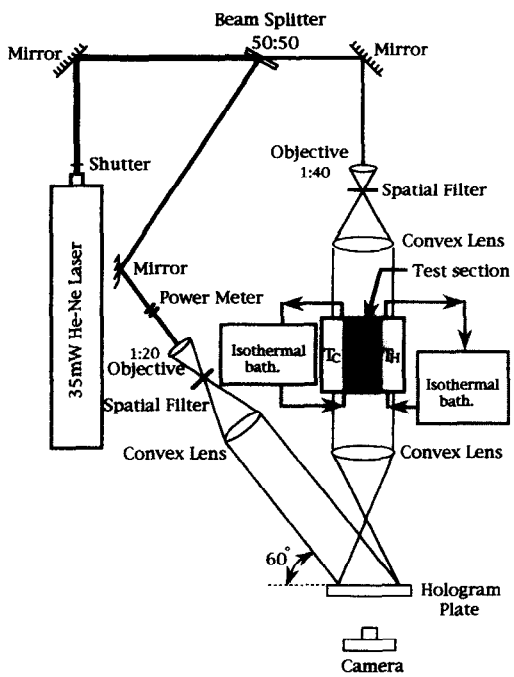

FIG. 3. Holographic interferometry for thermal field.

The length scales used in calculating the Nusselt and Rayleigh numbers are $H = 60(\pm 2\%)$, $100(\pm 1\%)$ and $200(\pm 0.5\%)$ mm, respectively. The temperature difference used in deriving the Rayleigh number is the difference in temperature of the hot and cold walls, i.e. the overall temperature difference. The major dimensionless parameters that determine the structure of a constant property flow in a differentially heated enclosure are the Rayleigh number,

$$Ra = \frac{g\beta\Delta T H^3}{\nu\alpha}, \tag{1}$$

the Prandtl number and the enclosure aspect ratios. The temperature difference used to calculate the heat transfer coefficient is the difference between the wall temperature and the mean bulk temperature:

$$Nu = \frac{hH}{k} \quad \text{and} \quad h = \frac{Q}{A_w |T_w - T_m|}. \tag{2}$$

A_w indicates the area used to derive the heat transfer coefficient, which is $60(\pm 2\%)$ $100(\pm 1.4\%)$ and $200(\pm 1.1\%)$ cm^2 for the present study. T_w stands for the temperature of the heated or cooled wall.

For each run, at least 12 h is needed to reach steady state. Steady state is indicated by a steady temperature difference (for constant flow rate) in the heating and cooling water for each wall. Cooling and heating water flow rates, nominally 680 kg h^{-1}, are measured with a rotameter. These were calibrated by a stop watch-and-bucket method to within $\pm 3\%$ for temperatures near ambient. The highest temperatures the walls operated at was about 80°C. The flow meter tended to read high by about 3–5% but, due to a decrease of approximately 2% in the fluid density, partially offsetting those two uncertainties is an error that increases about 3% at 25°C owing to the non-linearity of the temperature difference measuring period. Data are not corrected for conduction through the neoprene gasket from a heated wall to a cooled wall (about 5%), nor for radiation heat transfer from the hot wall to the cold wall (about 2%). The insulation effect was examined for the worst case (i.e. $\Delta T = 80$°C). It was found that the heat loss was about 5%. The overall heat balance in the test section (total measured heat transfer from hot wall minus total measured heat transfer to the cold wall divided by total measured heat transfer from the hot wall) was typically between $\pm 3\%$ (for the highest Rayleigh number) to $\pm 5\%$ (for the lowest Rayleigh number). In spite of this, the overall heat transfer measurements are expected to be within $\pm 5\%$ of the actual convection heat transfer from each wall. Based on the aforementioned relevant uncertainties, the maximum estimated uncertainties in *Ra* and *Nu* are 7% and 10%, respectively.

4. RESULTS AND DISCUSSION

The present study was conducted for $\Delta T = 0.5$–80°C with atmospheric air, distilled water and silicone

oil as the convective medium. The range of Ra varied from 8.7×10^2 to 2.0×10^9 and the local Prandtl number varied between 0.7 and 464. Five aspect ratios of $A = 1, 3, 5, 10$ and 20 with a fixed lateral aspect ratio $S = 5$ were studied. The lateral aspect ratio ($S = 5$) was chosen in an effort to minimize the end effect of the finite enclosure. The velocity for the present study is about 0.1–10 mm s^{-1}. Relevant geometrical parameters and variables concerned in the present measurements and calculations are listed in Table 1. For instance, the flow visualization was conducted for aspect ratios of enclosure of 3, 5, 10 and 20 for Prandtl number of 464 at $7.0 \times 10^8 \leqslant Ra \leqslant 2.0 \times 10^9$.

4.1. *Flow visualization*

The present results focus on the local steady-state behavior. To assist in explaining the local structure, flow visualization was made through a smoke-injection method under steady-state conditions. The steady-state conditions were determined when the variation of mean temperature of the vertical heated/cooled wall was $<0.5\%$ of that of its previous value. It usually takes 12 h to reach steady state. To elucidate the configuration of the flow field, observations have been made for vertical and horizontal cross-sections of the enclosures.

At the beginning, the interest was directed at understanding the flow in the center of the vertical plane of the enclosures. For this purpose observations of flow patterns and thermal fields were performed for a number of cases with increasing Rayleigh numbers (from 7.0×10^8 to 2.0×10^9). As an example, Fig. 4 shows the flow patterns at different planes for $A = 10$ and $Ra = 1.2 \times 10^9$. Figure 4(a) shows the flow field in the vertical mid-plane ($z = W/2$) of the enclosure. The effect of convection is clearly noted. Particles near the side walls closely follow the form of the enclosures. In the center, multi-cellular motion appears, surrounded by helical streamlines along which fluid is transported from the core to the adjacent walls. When the cells reach either the top or bottom end region they are totally destroyed. Strong end effects are shown due to large heat losses from the plexiglass walls, which were not insulated when conducting the flow visualization. Away from the ends, the flow is mainly vertical, with a slight periodic variation in the amplitudes of the vertical velocity. This periodicity of vertical velocity, together with that of the small transverse component, generates the aforementioned cellular stream pattern. Upon reaching the top or bottom wall, the main flow becomes two-dimensional and the cell disappears. Also obvious in the photograph is the waviness on the heated wall. The waves appear to break near the top or bottom of the enclosure. The waviness in the boundary layer occurred at the level of local Rayleigh numbers Ra_y, estimated to be 6×10^8, which coincides with that reported by Elder [13], who gives the condition for the onset of boundary layer waves as $Ra_y = 3 \times 10^8$ for aspect ratios between 9 and 17. Figure 4(b) shows the flow field in the horizontal top plane ($y = H$). This comfirms that the flow is nearly vertical and the boundary layer relaminarized after turning the top corner. Figure 4(c) presents the flow pattern in the horizontal mid-plane ($y = H/2$). It is clear that a relatively inactive core region exists. This phenomenon prevails for all the cases studied herein. Figure 5 represents the flow field in the vertical mid-plane ($z = W/2$), xz plane ($y = H$) and xz plane ($y = H/2$) of the enclosure for $A = 20$ at various Rayleigh numbers. Similarly, the effect of convection is clearly visible. At $Ra = 7.04 \times 10^8$, shown in Fig. 5(a), in the center of the vertical plane ($z = W/2$) one big vortex appears, surrounded by helical streamlines. The spiral flow pattern down the center of the enclosure indicates a spiraling motion from the front and back walls towards the center, and then a reverse spiral outside the central zone. As Ra increased to 9.2×10^8, the flow field was evaluated from photographs shown in Fig. 5(b) for the two-cell configuration. On further increases in the Rayleigh number, shown in Fig. 5(c), multi-cells appear and the flow becomes very complicated.

To observe the transition between one-cell and multi-cell systems, the Rayleigh number was changed gradually from 7.04×10^8 to 2.0×10^9 by changing the temperature difference ΔT between the heated and cooled walls (see Fig. 5). At small temperature differences in terms of the Rayleigh number, as stated above, only one cell is observed in the vertical mid-plane of the enclosure. The center of this cell is not in the middle of the plane (parallel to heated or cooled vertical wall) but is moved toward the cooled wall. At higher Rayleigh number ($Ra = 9.2 \times 10^8$), a second cell appears in the plane of symmetry that has the same result of rotation as the first cell. On this occasion, the stream bends in toward the plane of symmetry and impinges the heated wall normally prior to being entrained into the boundary layer and flowing

Table 1. Relevant geometrical parameters and variables concerned in the present measurements and calculations

	Aspect ratio (A)	Prandtl number (Pr)	Rayleigh number (Ra)
Flow visualization	3, 5, 10, 20	464	7.0×10^8–2.0×10^9
Thermal visualization	1, 3, 5	0.7	8.7×10^2–1.5×10^4
Temperature distribution	3, 5	0.7, 6	1.6×10^6–7.5×10^8
Nusselt number	3, 5, 10	0.7, 6, 464	1.0×10^6–2.0×10^9

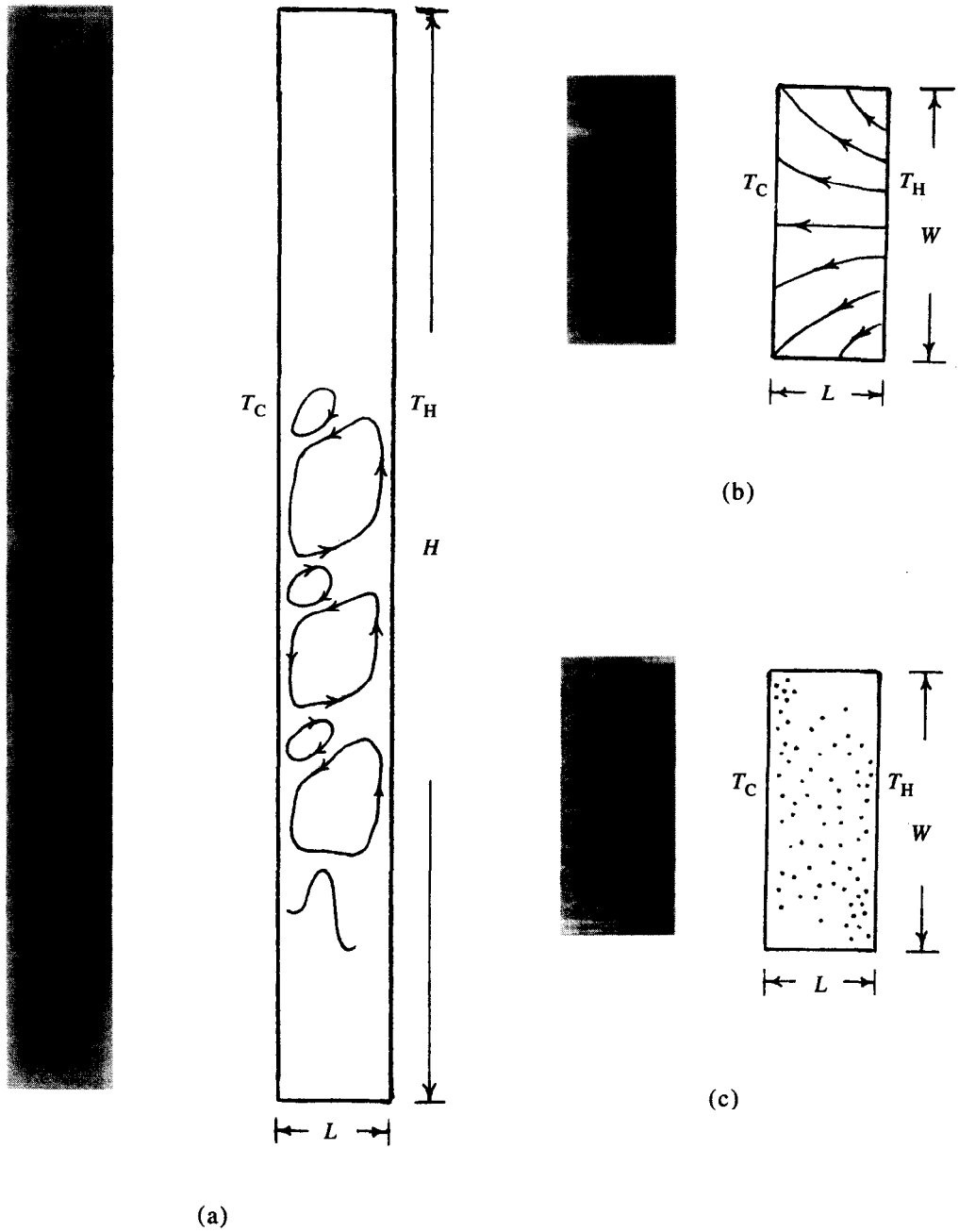

FIG. 4. Flow visualization ($Pr = 464$) for $A = 10$, $Ra = 1.2 \times 10^9$ at different planes. (a) xy plane, $z = W/2$. (b) xz plane, $y = H$. (c) xz plane, $y = H/2$.

upward. From the junction of the wall and the top ceiling, the stream proceeds across the top ceiling in a similar curved path until it reaches the cooled wall, where it flows downward with the wall boundary layer. Weak cellular structures were observed in the core near the top ceiling. This can also be seen from Fig. 5 in the xz plane and $y = H$. Furthermore, for all three Rayleigh numbers considered, in the xz plane and with $y = H/2$, it is found that the flow in the core is almost stagnant. Examination of the perspective three-dimensional fields (not shown) revealed that the variations in the z-direction were evident, particularly near the front/back walls ($Z = 0$ and W). As the Rayleigh number increases, convection activity intensifies and significant three-dimensional effects exist in narrow areas near the front/back walls.

In summary, the flow visualization results indicate that the inactive core does not play an important role in transferring heat from the heated wall to the cooled wall. The heat transfer is accomplished almost entirely by flow in the boundary layers up the heated wall, across the top ceiling and down the cooled wall. Three-dimensional effects were found near side walls and become significant as the Rayleigh number increases.

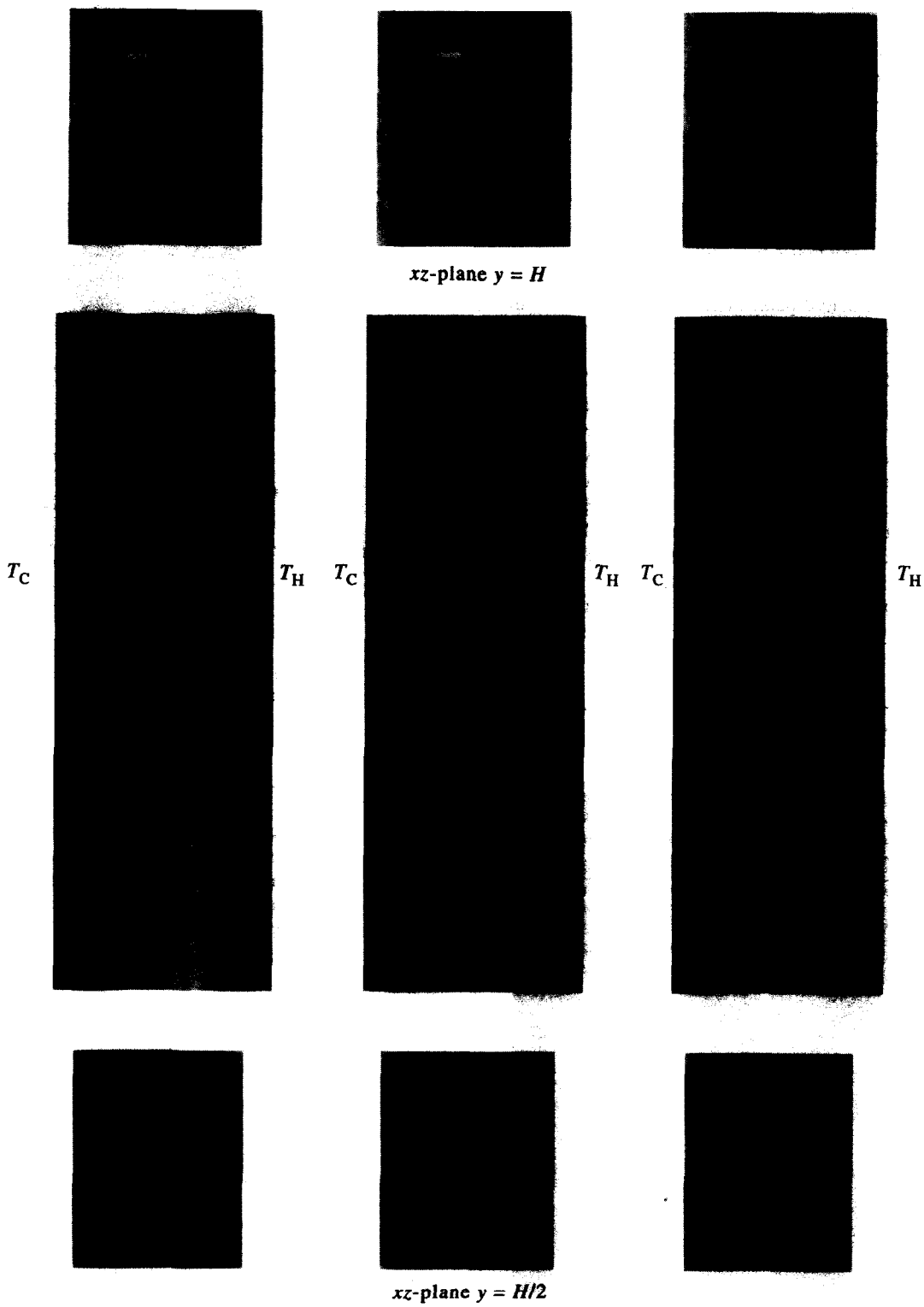

FIG. 5. Flow visualization ($Pr = 464$) for $A = 20$ at various Rayleigh numbers. (a) $Ra = 7.04 \times 10^8$. (b) $Ra = 9.2 \times 10^8$. (c) $Ra = 2.0 \times 10^9$.

4.2. *Thermal visualization*

The interferograms of the temperature field in the infinite fringe mode in the vertical mid-plane with $Ra = 8.7 \times 10^2$, 1.3×10^3 and 1.5×10^4 for $A = 5$ are presented in Fig. 6. The isotherms are deformed by convection into the characteristic S-shape for temperature inversion as the Rayleigh number increases. Figure 7 presents thermal visualization at $Ra = 5.4 \times 10^3$ for aspect ratios of $A = 1$, 3 and 5. Figure 7(a) illustrates the core temperature of the enclosure and reveals stratification with a nearly linear vertical temperature distribution and weak variations in a horizontal plane. This behavior becomes dominant as the aspect ratio decreases. This coincides with previous work in two dimensions [14]. It is not surprising that only minor three-dimensional effects have been noted due to a fairly large lateral aspect ratio ($S = 5$). This tends to reduce the three-dimensional effects. The temperature field is linearly stratified in the vertical direction and is practically independent of the distance away from the wall, except for a thin region near the heated wall where a sharp thermal boundary layer exists. Three-dimensionalities are prominent only near the thin region (i.e. near the side walls). This fluid region is the continuation of the hot fluid jet traveling upward along the heated vertical wall and it spreads along the top ceiling. Far away from the heated wall the existence of the hot fluid region is not felt. Based on the photographs of thermal visualization (Figs. 6 and 7), it is found that the temperature field inside the enclosure consists of an 'active' region and an 'inactive' region. In the active region, vivid flow motion provides convection as the dominant heat transfer mechanism. The active region occupies a small part of the enclosure which is near the vicinity of the heated wall and horizontal walls. The inactive region constitutes the remainder of the enclosure. In this region heat transfer is dominated by conduction. However, this phenomenon becomes more significant as the Rayleigh number increases and the aspect ratio increases for the cases under study.

FIG. 7. Thermal visualization ($Pr = 0.7$) for $Ra = 5.4 \times 10^3$ at various aspect ratios.

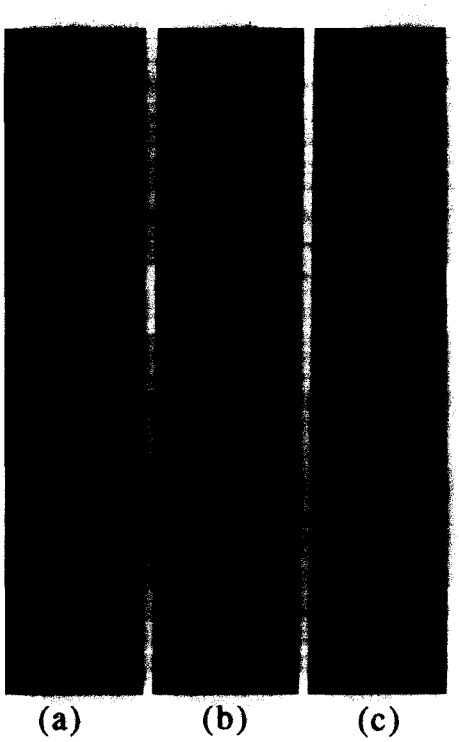

FIG. 6. Thermal visualization ($Pr = 0.7$) for $A = 5$ at various Rayleigh numbers. (a) $Ra = 8.7 \times 10^2$. (b) $Ra = 1.3 \times 10^3$. (c) $Ra = 1.5 \times 10^4$.

4.3. *Temperature distribution*

The vertical temperature distribution in the core of the enclosure was obtained because the stable thermal stratification significantly influences the boundary layer flows. In Fig. 8, the dimensionless core tem perature $(T - T_C/T_H - T_C)$ at three vertical positions for various values of Rayleigh number is presented. Figures 8(a) and (b) display linear temperature distributions across the core of the enclosure, which indicates that heat from the heated wall to the cooled wall is transported by conduction through the major portion of the core, and by convection at the bottom of the heated wall and the top of the cooled wall. This is evidenced by previous thermal visualization for Fig. 6. As the Rayleigh number increases, convection dominates and, furthermore, temperature inversions

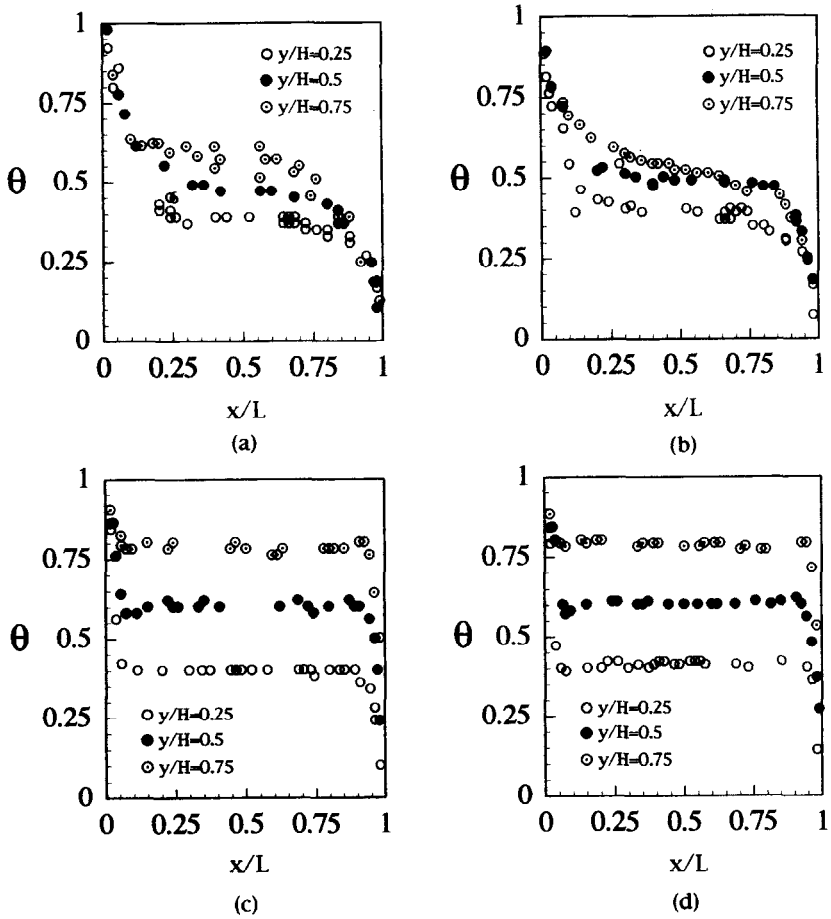

FIG. 8. Temperature profile at various vertical positions for $A = 3$. (a) $Ra = 1.60 \times 10^6$. (b) $Ra = 3.20 \times 10^6$. (c) $Ra = 3.77 \times 10^8$. (d) $Ra = 7.53 \times 10^8$.

were observed in the center portions shown in Figs. 8(c) and (d). These inversions suggest that the flow immediately adjacent to the vertical walls is so strong that it produces a high rate of tangential convection along the heated wall compared to the vertical transport of heat from the surface of heated wall across to the cooled wall. At this stage, simultaneous conduction in the core of the enclosure is actually opposite to the overall direction of heat flow. This behavior verifies the previous flow visualization shown in Figs. 4 and 5 in which multi-cells occur in the core at higher Rayleigh numbers.

Figure 9 presents the temperature profile at $Ra = 3.7 \times 10^8$ when $A = 5$ at three different elevations for three different working fluids. As mentioned in Elder's work [13] for large Prandtl numbers, temperature inversions occurred at moderate Prandtl numbers ($Pr = 0.7$, 6 and 464) in the present study. The Prandtl number effects shown in Fig. 9 were notable for the thinner thermal boundary layers for higher Prandtl numbers.

In summary, the presence of core stratification and its effect on the flow pattern is more pronounced at higher Rayleigh numbers. Consider, for instance, the upward flow on the heated wall. Hot fluid flowing in the boundary layer finds itself in an environment (core) having a higher temperature. The temperature of the outer portion of the boundary layer 'lags' behind that of the stratified core. This is often referred to in the literature as a 'temperature defect' in the flow. This results in flow reversal in the outer portion of the boundary layer, which is also evidenced by flow visualization. Similar statements hold for the case of the downward boundary layer flow on the cooled wall. Furthermore, the Prandtl number effect was found to be significant for the cases under study.

4.4. *Nusselt number correlation*

The Nusselt number as a function of Ra is presented in Figs. 10 and 11. For simplicity, the current results permit the identification of only two regimes of heat transfer, which are the laminar and turbulent (plus transition) regimes. Through multiple regression analysis, it is found that:

$$Nu = 0.321 Ra^{0.241} A^{-0.095} Pr^{0.053}$$

(for the laminar regime) (3)

and

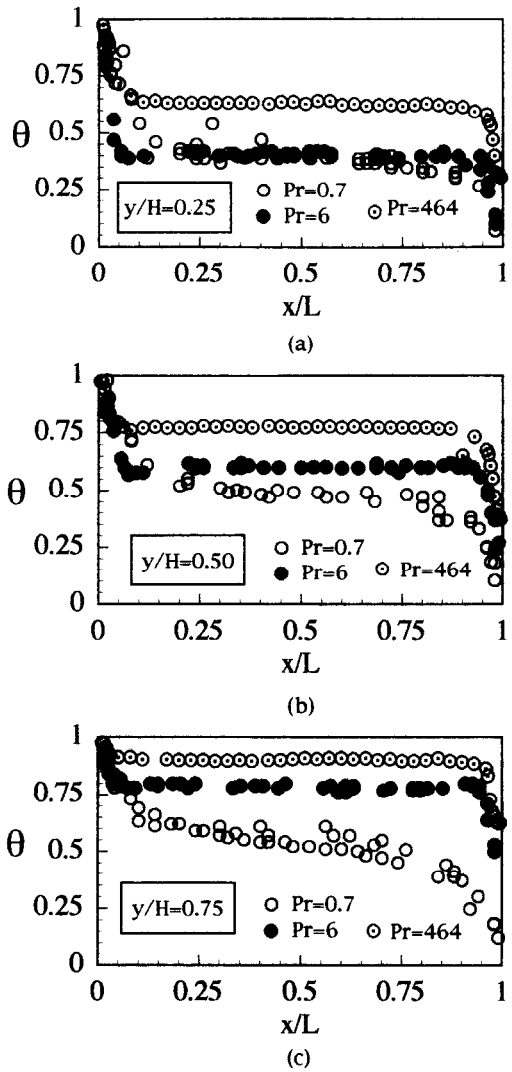

FIG. 9. Temperature profile for $A = 5$ and $Ra = 3.7 \times 10^8$. (a) $y/H = 0.25$. (b) $y/H = 0.50$. (c) $y/H = 0.75$.

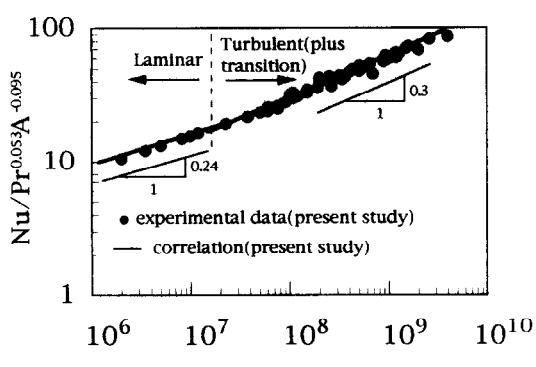

FIG. 10. *Nu* vs *Ra*.

$$Nu = 0.133 Ra^{0.301} A^{-0.095} Pr^{0.053}$$

(for the turbulent plus transition regime) (4)

within $\pm 10\%$ of the experimental data. The *Nu* data correlate well with a nearly 1/4 power of *Ra*, as predicted from laminar boundary layer theory [3]. The regression analysis further shows that the heat transfer mechanism is laminar convection closing vertical walls surrounding the core region when $Ra \leqslant 1.4 \times 10^7$, as shown in Fig. 11. This also confirms the preceding thermal visualization and two-dimensional flow discussed by previous investigators [13] and the findings reported from ref. [10] for three-dimensional laminar natural convection in an enclosure where $1 \times 10^4 \leqslant Ra \leqslant 2 \times 10^7$. However, when $Ra > 1.4 \times 10^7$, based on the present study, it is found that a substantial portion of the wall boundary layer becomes turbulent. This waviness was observed in the preceding flow visualization, which results in an $Ra^{1/3}$ dependence. This coincides with the results found by a scale analysis [3]. The large exponent of *Ra* indicates a strong contribution of convection to the overall heat transfer. Since the heat transfer mechanism is almost boundary layer convection, the boundary layer flow is not disturbed by the presence of adjacent walls and is thus configuration independent. This can be seen from the power of -0.095 found for the aspect ratio. This agrees reasonably well with previous studies [1, 2, 5]. For comparison, several previous two-dimensional studies were plotted with the present turbulent results in Fig. 12 and the comparison can be seen to be quite favorable in both tendency and magnitude. Large deviation occurred at large Prandtl number ($Pr \cong 464$). Furthermore, for Rayleigh numbers smaller than 3×10^8, the three-dimensional Nusselt numbers are found to be appreciably higher than those for the two-dimensional results. However, at $Ra = 10^9$, the difference is considerably smaller. Consequently, it is speculated that three-dimensional effects are prominent when $Ra \leqslant 3 \times 10^8$ for the present study.

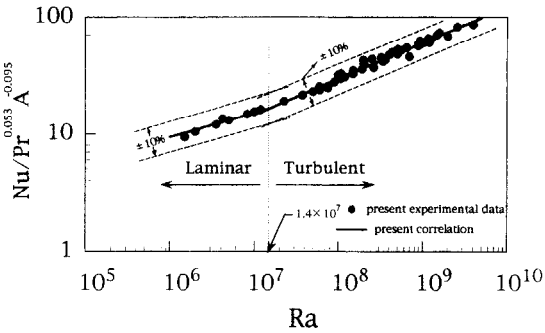

FIG. 11. The deviation of the present correlation with experimental data.

5. CONCLUSIONS

Flow/thermal visualization experiments and heat transfer measurements have been completed for three-dimensional natural convection in rectangular enclosures at Rayleigh numbers of 8.7×10^2–2.0×10^9 with three different working fluids. The test cell had one

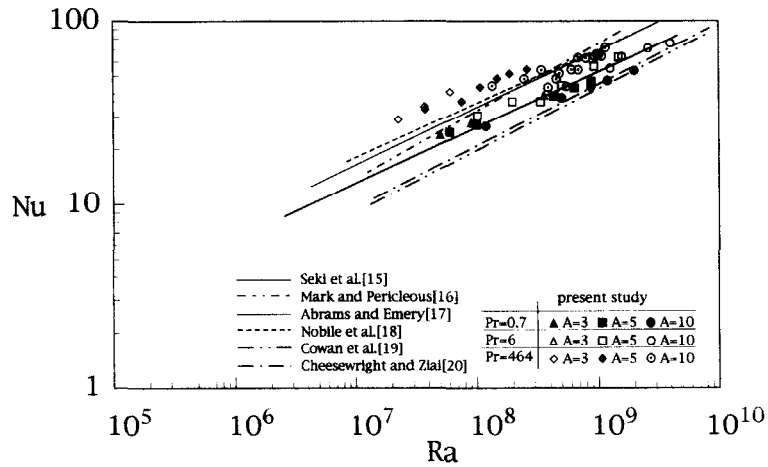

FIG. 12. Comparison of the present results with those of previous studies.

heated and cooled vertical wall. The four remaining walls were adiabatic. The most significant contributions of the present study are the following.

(1) Experiments show that convection in rectangular enclosures has an intrinsically three-dimensional character and the flow visualization experiments verify the existence of a relatively inactive core surrounded by boundary layers on each of the four vertical walls. Transport of heat from the heated wall to the cooled wall is carried out by flow in the boundary layers. The streamline reveals that the characteristic co-axial double spiral movement towards the center plane occurs when $Ra \leqslant 7.04 \times 10^8$.

(2) Transition to turbulent flow was observed for higher Ra ($Ra > 1.4 \times 10^7$) from both flow visualization and Nusselt number correlation. Three-dimensional effects are significant at higher Ra and larger aspect ratio ($A \geqslant 5$).

(3) Thermal visualization provides additional proof for the results that throughout most of the enclosure the temperature field is practically two-dimensional, linearly stratified in the vertical except for the regions near the four side walls. The circulation pattern within the enclosure became clear as Rayleigh number and aspect ratio increased. Three-dimensional effects exist near the side walls. The size of the area where three-dimensionalities are dominant becomes smaller as the Rayleigh number increases.

(4) Bifurcation was identified for the laminar and turbulent (plus transition) regimes at $Ra = 1.4 \times 10^7$. Correlations were made for these two regions and verified by a two-dimensional scale analysis. They are

$$Nu = 0.321 Ra^{0.241} A^{-0.095} Pr^{0.053} \quad (Ra \leqslant 1.4 \times 10^7)$$

$$Nu = 0.133 Ra^{0.301} A^{-0.095} Pr^{0.053} \quad (Ra > 1.4 \times 10^7).$$

The correlations indicate that there is a laminar and turbulent (plus transition) boundary layer flow heat transfer mechanism in the present study.

(5) Aspect ratio effects on heat transfer were not clearly noted for all the cases under study. However, the results for Prandtl number effects suggest that the heat transfer mechanism is convection in the boundary layers that are affected by the different core flow set up for the different working fluids.

Acknowledgements—This work was supported in part by a research grant from China Petroleum Company (Taiwan, R.O.C.) for which the authors express their sincere gratitude. Assistance in the preparation of the revised manuscript from Mr Shi-Chiang Young is greatly appreciated.

REFERENCES

1. S. Ostrach, Natural convection in enclosures, *Adv. Heat Transfer* **8,** 161–227 (1972).
2. S. Ostrach, Natural convection in enclosures, *ASME J. Heat Transfer* **110,** 1175–1190 (1988).
3. A. Bejan, *Convection Heat Transfer*, pp. 159–201. Wiley, New York, (1984).
4. D. Poulikakos and A. Bejan, Natural convection experiments in a triangular space, *ASME J. Heat Transfer* **105,** 652–655 (1983).
5. A. Zebib, G. Schubert and J. Strauss, Infinite Prandtl number thermal convection in a spherical shell, *J. Fluid Mech.* **91,** 257–277 (1980).
6. G. de Vahl Davis, Laminar natural convection in an enclosed rectangular cavity, *Int. J. Heat Mass Transfer* **11,** 1675–1693 (1968).
7. T. Fusegi, J. M. Hyun, K. Kuwahara and B. Farouk, A numerical study of three-dimensional natural convection in a differentially heated cubical enclouse, *Int. J. Heat Mass Transfer* **34,** 1543–1557 (1991).
8. A. Gadgil, F. Banmon and R. Kammerud, Natural convection in passive solar buildings : experiments, analysis, and results, *Passive Solar J.* **1,** 28–40 (1982).
9. D. Sadowski, D. Poulikakos and M. Kazmierczak, Three-dimensional natural convection experiments in an enclosure, *J. Thermophys.* **2,** 242–249 (1988).
10. W. J. Hiller, S. Koch and T. A. Kowalewski, Three-dimensional structures in laminar natural convection in a cubic enclosure, *Exp. Therm. Fluid Sci.* 2, 33–44 (1989).
11. A. M. Lankhorst, D. Angirasa and C. J. Hoogendoorn, LDV measurements of buoyancy-induced flows in an enclosure at high Rayleigh numbers, *Exp. Therm. Fluid Sci.* **1,** 74–79 (1993).
12. W. Aung and R. O'Regan, Precise measurement of heat transfer using holographic interferometry, *Rev. Scient. Instrum.* **42,** 1755–1758 (1971).

13. J. W. Elder, Turbulent free convection in a vertical slot, *J. Fluid Mech.* **23,** 99–111 (1965).
14. G. K. Batchelor, Heat transfer by free convection across a closed cavity between boundaries at different temperatures, *Q. Appl. Math.* **12,** 209–233 (1954).
15. N. Seki, S. Fukusako and H. Inaba, Visual observation of natural convection flow in a narrow vertical cavity, *J. Fluid Mech.* **89,** 695–704 (1978).
16. N. C. Mark and K. A. Pericleous, Laminar and turbulent natural convection in an enclosed cavity, *Int. J. Heat Transfer* **27,** 755–772 (1984).
17. A. Abrams and A. F. Emery, Turbulent free convection in square cavities with mixed boundary conditions, *Heat Transfer in Convective Flows* **107,** 117–127 (1989).
18. E. Nobile, A. C. M. Sousa and G. S. Barozzi, Turbulent bouyant flow in enclosures, *Proc. 9th Int. Heat Transfer Conf.* **5,** 543–548 (1990).
19. G. H. Cowan, P. G. Lovegrove and G. L. Quarini, Turbulent natural convection heat transfer in vertical single water-filled cavities, *Proc. 7th Int. Heat Transfer Conf.* **2,** 195–203 (1982).
20. R. Cheesewright and S. Ziai, Distributions of temperature and local heat-transfer rate in turbulent natural convection in a large cavity, *Proc. 8th Int. Heat Transfer Conf.* **4,** 1465–1470 (1986).